Nuclear dependence in direct photon production

Xiaofeng Guo and Jianwei Qiu

Department of Physics and Astronomy, Iowa State University, Ames, Iowa 50011

We calculate the nuclear dependence of direct photon production in hadron-nucleus collisions. In terms of a multiple scattering picture, we factorize the cross section for direct photon production into calculable short-distance partonic parts times multiparton correlation functions in nuclei. We present the hadron-nucleus cross section as A^α times the hadron-nucleon cross section. Using information on the multiparton correlation functions extracted from photon-nucleus experiments, we compute the value of α as a function of transverse momentum of the direct photon. We also compare our results with recent data from Fermilab experiment E706. [S0556-2821(96)05211-3]

I. INTRODUCTION

As early as in 1970s, it was observed [1] that inclusive cross sections for single high-transverse-momentum particles produced in hadron-nucleus scattering show an ''anomalous'' nuclear dependence, in which the cross section at fixed transverse momentum grows approximately as A^α, with A the atomic number of the nuclear target. The value of α is a function of the transverse momentum, and can be as large as 4/3. This phenomenon has been known as the Cronin effect. The typical energy exchange in a high-transverse-momentum scattering process is so large that any single hard scattering should be very localized within a single nucleon. Consequently, a linear A dependence is expected for single scattering processes. Therefore, the Cronin effect is often described as due to multiple scattering of partons in nuclear matter [2–5]. The $A^{4/3}$ behavior signals a dependence on nuclear size, and multiple scattering is dominated by double scattering.

In some of the previous work on this topic, an independent scattering picture was adopted [2]. In this picture, each scattering was treated independently. For example, the cross section for double scattering was proportional to a product of two Born cross sections. The double scattering cross section in this picture is not infrared safe, however. This is because the kinematics of single particle inclusive cross sections can only provide a constraint on the total momentum from the target, which leaves the possibility that one of the Born cross section diverges when the momentum transfer of this Born cross section approaches zero. Therefore, theoretical predictions from the independent scattering picture are sensitive to the infrared cutoffs which must be introduced in the calculations.

Recently, Luo, Qiu, and Sterman (LQS) have shown that the anomalous nuclear enhancement can be described naturally in perturbative QCD, in terms of a nonleading power or ''higher-twist'' formalism [5]. In this treatment, the contribution from double scattering can be factorized into short-distance hard parts convoluted with corresponding multiparton matrix elements or multiparton correlation functions in nuclei. The short-distance partonic parts are calculable in perturbative QCD, and all infrared divergences associated with soft rescatterings in perturbation theory can systemati-

cally be absorbed into multiparton correlation functions. The multiparton correlation functions are nonperturbative, just like the parton distributions in the single scattering processes. These correlation functions in nuclei provide information about nuclear matter and its interaction with high-energy probes. They can reveal information different from what normal parton distributions in nuclei can provide, and in principle, they are as fundamental as the parton distributions. In order to test the theory, we need to find different processes which depend on the same multiparton correlation functions. Information on these new correlation functions extracted from one set of processes may be applied in other processes.

Our aim in this paper is to show that the consistent perturbative QCD treatment of double scattering developed by LQS can be naturally applied to high-transverse-momentum direct photon production in hadron-nucleus scattering. We factorize the cross section of direct photon production into calculable short-distance partonic parts times multiparton correlation functions, which are the same as those derived in Ref. [5]. We calculated the short-distance partonic hard parts. We evaluate the nuclear dependence by using the information on multiparton correlation functions, extracted from experiments on the momentum imbalance of two-jet photoproduction on nuclear targets [5]. Our numerical results are consistent with recent measurements of the nuclear dependence in direct photon production from Fermilab E706 experiments [6].

A double scattering with high momentum transfer must have at least one hard scattering to produce the high-transverse-momentum observables. In addition, there may be a soft scattering either before or after the hard scattering (referred to below as a soft-hard process) or another hard scattering (called a double hard process). We shall show that only the soft-hard processes contribute to the nuclear dependence of direct photon production to the order we consider. The fact that the photon does not interact strongly once produced at the hard collisions eliminates final-state multiple scattering in direct photon cross sections. Therefore, direct photon production in hadron-nucleus scattering provides an excellent test of initial-state multiple scatterings, while jet or single particle production in photon-nucleus scattering provides independent tests of final-state multiple scatterings. Jet

and single particle production in hadron-nucleus collisions, on the other hand, receive contributions from both initial- and final-state multiple scatterings. Final-state multiple scattering in photoproduction has been discussed in Ref. [5]. Our work will provide the complementary information on the initial-state multiple scattering.

We begin in Sec. II with an outline of the formalism used in our calculation. Complete analytical results of our calculation are also presented in Sec. II. The detailed derivation of our results and the calculation of the partonic hard parts are presented in Sec. III. In Sec. IV, we present our numerical results. We also compare our numerical results with recent experimental data. We conclude with a brief summary and suggestions for further work.

II. FORMALISM AND ANALYTICAL RESULTS

An energetic photon can be directly produced at short distance in high-energy collisions, and does not interact strongly once produced. Therefore, it has been recognized for a long time that direct photon production is a clean probe for short-distance dynamics in high-energy collisions [7]. Data from hadronic prompt photon production play a very important role in QCD global analysis, and provide constraints on gluon distributions in hadrons [8–10]. In this section, we outline the general formulas for cross sections of direct photon production, and present our analytical results for the contribution from double scattering processes.

A. Formalism

In the following discussion, we study direct photon production in hadron-nucleus collisions:

$$h(p') + A(p) \rightarrow \gamma(l) + X, \qquad (1)$$

where p is defined as the averaged momentum per nucleon. In general, the total cross section for the above process can be expressed as a sum of contributions from single scattering, double scattering, and even higher multiple scattering:

$$d\sigma_{hA \rightarrow \gamma}(l) = d\sigma_{hA \rightarrow \gamma}^{(S)}(l) + d\sigma_{hA \rightarrow \gamma}^{(D)}(l) + \cdots, \qquad (2)$$

where the superscripts (S) and (D) represent the single and double scattering, respectively, and the ellipsis represents other possible multiple scatterings. In this paper, we consider only double scattering, and its contribution to the nuclear dependence.

As a result of perturbative factorization [11], the single scattering cross section can be expressed as

$$d\sigma_{hA \rightarrow \gamma}^{(S)}(l) = A d\sigma_{hN \rightarrow \gamma}^{(S)}(l)$$

$$= A \sum_{a,b} \int dx' f_{a/h}(x')$$

$$\times \int dx f_{b/N}(x) d\hat{\sigma}_{ab \rightarrow \gamma}(x', x, l). \qquad (3)$$

In Eq. (3), $f_{a/h}(x')$ is a normal parton distribution in the beam hadron h and $f_{b/N}(x)$ is an effective nucleon parton distribution inside a nucleus, which should include the well-known European Muon Collaboration (EMC) effect. In prin-
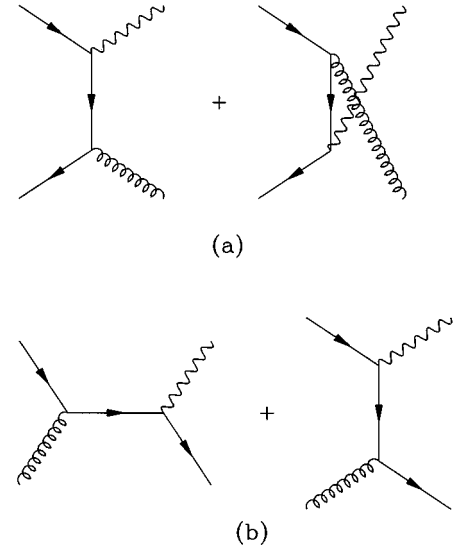

FIG. 1. Lowest-order Feynman diagrams contribute to single scattering: (a) ''annihilation'' and (b) ''Compton.''

ciple, the parton-parton scattering cross section $d\hat{\sigma}_{ab \rightarrow \gamma}$ should include both direct and fragmentation contributions. That is, an energetic photon can be produced directly at short distances or produced from the fragmentation of an energetic parton which was produced at short distances [7,12]. For example, partonic scattering may produce an energetic quark, which radiates a photon. Since we are most interested in fixed target experiments here, the fragmentation contribution is much smaller than the direct contribution in most of phase space [12]. Therefore, in the rest of our discussion, we will consider only direct production of photons. For example, at the lowest order, we have contributions from $q\bar{q} \rightarrow \gamma g$ ''annihilation'' diagrams, sketched in Fig. 1(a), and $gq(\text{or } \bar{q}) \rightarrow \gamma q(\text{or } \bar{q})$ ''Compton'' diagrams, sketched in Fig. 1(b).

In terms of the generalized factorization theorem [13], the double scattering cross section can be written as

$$d\sigma_{hA \rightarrow \gamma}^{(D)}(l) = \sum_{a} \int dx' f_{a/h}(x') d\sigma_{aA \rightarrow \gamma}^{(D)}(x', p, l), \quad (4)$$

where $d\sigma_{aA \rightarrow \gamma}^{(D)}(x', p, l)$ can be thought as the double scattering cross section between a parton and the nucleus. At the lowest order, it can be factorized as

$$d\sigma_{aA \rightarrow \gamma}^{(D)}(x', p, l) = \int dx \, dx_k \, dx_{k'} \sum_{\{i\}} T_{\{i\}}(x, x_k, x_{k'})$$

$$\times H_{\{i\}}(x', x, x_k, x_{k'}, l). \qquad (5)$$

In Eq. (5), $T_{\{i\}}(x, x_k, x_{k'})$ are the matrix elements of four-parton operators, characterized by the set of fields operators $\{i\}$, and $H_{\{i\}}$ are the corresponding partonic hard scattering functions. The x, x_k, and $x_{k'}$ are independent collinear momentum fractions carried by the partons from the nucleus. The graphical representation of Eq. (5) is shown in Fig. 2. At the lowest order, there are three types of partonic subprocesses that contribute to the double scatterings. Feynman diagrams of these partonic subprocesses are sketched in Fig. 3.
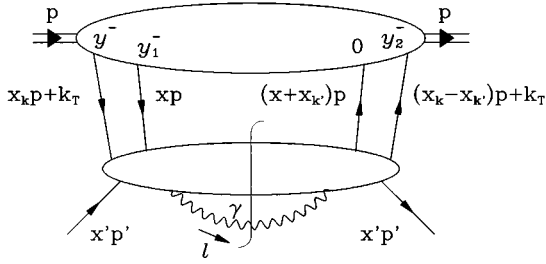
FIG. 2. A graphical representation of double scattering contributions from the parton-nucleus collisions.

We define the invariant direct photon cross section in hadron-nucleus collisions in terms of cross sections in hadron-nucleon collisions:

$$
E_l \frac{d\sigma_{hA\to\gamma}(l)}{d^3l} \equiv A^{\alpha(l)} E_l \frac{d\sigma_{hN\to\gamma}^{(S)}(l)}{d^3l}
$$

$$
\approx E_l \frac{d\sigma_{hA\to\gamma}^{(S)}(l)}{d^3l} + E_l \frac{d\sigma_{hA\to\gamma}^{(D)}(l)}{d^3l}, \quad (6)
$$

where Eq. (2) was used. Substituting Eq. (3) into Eq. (6), we obtain the definition for the nuclear dependence parameter $\alpha(l)$:
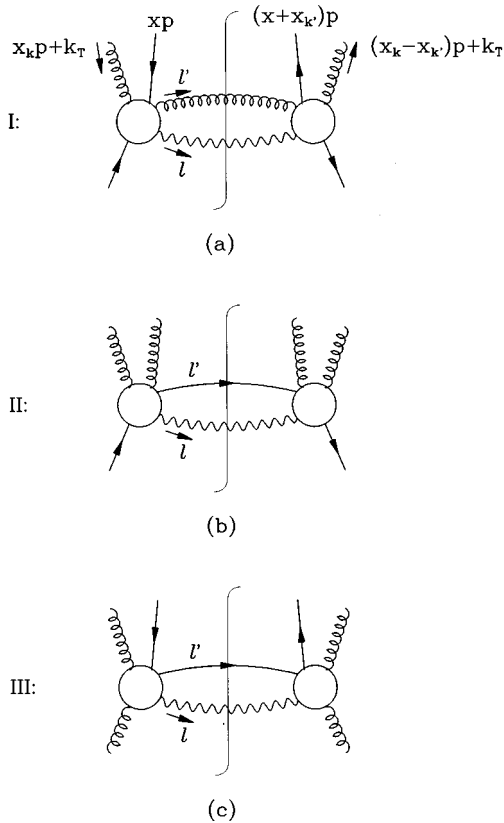

FIG. 3. Three types of leading order Feynman diagrams contribute to the double scattering. (a) Type I, ''annihilation'' diagrams corresponding to the two-quark–two-gluon matrix element; (b) Type-II, ''Compton'' diagrams corresponding to the four-gluon matrix element; (c) Type-III, ''Compton'' diagrams corresponding to the two-quark–two-gluon matrix element.

$$
\alpha(l) = 1 + \frac{1}{\ln(A)} \ln\left(1 + \frac{1}{A} \frac{E_l d\sigma_{hA\to\gamma}^{(D)}(l)/d^3l}{E_l d\sigma_{hN\to\gamma}^{(S)}(l)/d^3l} \right). \quad (7)
$$

From Eq. (7), $\alpha(l) > 1$ if $d\sigma_{hA\to\gamma}^{(D)}/d^3l$ is positive, which will turn out to be the case for the kinematic regime in which we are interested here. However, in general, the double scattering contribution $\sigma^{(D)}$ may be negative, and $\alpha(l) < 1$ in a certain part of phase space. The positivity of a cross section requires the sum of all possible multiple scattering contributions to be positive. The separation between single and double scatterings is not unique. For example, two scatterings can be very close to each other and localized in one nucleon, and such a double scattering will not provide the anomalous nuclear dependence and may be classified as a single scattering.

We will argue later that the leading double scattering contribution $d\sigma_{hA\to\gamma}^{(D)}/d^3l$ is proportional to $A^{4/3}$. Consequently, the value of $\alpha(l)$ will be between 1 and 4/3, depending on the relative sizes of contributions from the single and double scatterings. If the double scattering contribution is larger than the single scattering contribution in a certain part of the phase space, the value of $\alpha(l)$ in that region will approach 4/3.

B. Analytic results

In this subsection, we present the analytic results which are used to calculate the nuclear dependence parameter $\alpha(l)$ defined in Eq. (7).

Following Eq. (3), the lowest-order invariant cross section for single scattering direct photon production is given by [7]

$$
E_l \frac{d\sigma_{hN\to\gamma}^{(S)}(l)}{d^3l} = \sum_{a,b} \int dx' f_{a/h}(x')
$$

$$
\times \int dx f_{b/N}(x) \delta\left(x - \frac{-x't}{x's+u} \right)
$$

$$
\times \alpha_{em}\alpha_s \left(\frac{1}{\hat{s}} \right)\left(\frac{1}{x's+u} \right) |\bar{M}_{ab\to\gamma}|^2, \quad (8)
$$

where $\Sigma_{a,b}$ run over all gluon, quark, and antiquark flavors, and the matrix elements for the ''annihilation'' and ''Compton'' subprocesses, sketched in Fig. 1, are given by

$$
|\bar{M}_{q\bar{q}\to\gamma g}|^2 = e_q^2 \left(\frac{4}{9} \right) 2\left(\frac{\hat{u}}{\hat{t}} + \frac{\hat{t}}{\hat{u}} \right), \quad (9a)
$$

$$
|\bar{M}_{qg\to\gamma q}|^2 = e_q^2 \left(\frac{1}{6} \right) 2\left(\frac{-\hat{t}}{\hat{s}} + \frac{\hat{s}}{-\hat{t}} \right), \quad (9b)
$$

where e_q is the fractional charge carried by a quark of type ''q.'' The invariants $\hat{s}$, $\hat{t}$, and $\hat{u}$ are the usual Mandelstam invariants for the parton-parton subprocess. They are related to those at the hadron-nucleon interaction by

$$
\hat{s} = x'xs, \quad \hat{t} = x't, \quad \hat{u} = xu, \quad (10a)
$$

$$
s = (p'+p)^2, \quad t = (p'-l)^2, \quad u = (p-l)^2. \quad (10b)
$$

In the case of double scattering, there are four physical partons linking the matrix elements T and the partonic hard parts H, as shown in Eq. (5). After taking into account momentum conservation, there are still *three* independent momentum fraction integrations (x, x_k, and $x_{k'}$ defined in Fig. 2) between the matrix elements and the partonic parts, in contrast to *one* independent momentum fraction integration

for the case of single scattering. As explained in next section, we take the leading pole approximation to integrate over two of the three momentum fractions (e.g., x_k and $x_{k'}$). Then, the invariant double scattering cross section $E_l d\sigma_{hA\to\gamma}^{(D)}/d^3 l$ can be reduced into a form very similar to the single scattering cross section defined in Eq. (8). Following our derivation in next section, we obtain

$$E_l \frac{d\sigma_{hA\to\gamma}^{(D)}(l)}{d^3 l} = \alpha_{em}(4\pi\alpha_s)^2 \int dx' dx \, \delta\left(x - \frac{-x't}{x's+u}\right)\left(\frac{1}{x's}\right)\left(\frac{1}{x's+u}\right)\sum_q e_q^2[f_{\bar{q}/h}(x')\Phi_q(x,x',A)H_{q\bar{q}}$$

$$+ f_{q/h}(x')\Phi_g(x,x',A)H_g + f_{g/h}(x')\Phi_q(x,x',A)H_q], \tag{11}$$

where $\sum_q$ runs over all quark and antiquark flavors. In Eq. (11), the functions Φ_i with $i=q,g$ represent the effective parton flux from the nucleus. They are given by

$$\Phi_i = \left[\frac{\partial^2}{\partial x^2}\left(\frac{T_i(x,A)}{x}\right)\right]\left(\frac{l_T^2}{(x's+u)^2}\right) + \left[\frac{\partial}{\partial x}\left(\frac{T_i(x,A)}{x}\right)\right]\left(\frac{-u}{x's(x's+u)}\right). \tag{12}$$

The $T_i(x,A)$ with $i=q,g$ in Eq. (12) are the twist-4 matrix elements in nuclei. They were originally introduced in Ref. [5], and are given by

$$T_q(x,A) = \int \frac{dy_1^-}{2\pi} e^{ixp^+y_1^-} \int \frac{dy^- dy_2^-}{2\pi} \theta(y_1^- - y^-)\theta(-y_2^-)\frac{1}{2}\langle p_A | F_\alpha^{+}(y_2^-)\bar{\psi}_q(0)\gamma^+\psi_q(y_1^-)F^{+\alpha}(y^-)|p_A\rangle \tag{13a}$$

and

$$T_g(x,A) = \int \frac{dy_1^-}{2\pi} e^{ixp^+y_1^-} \int \frac{dy^- dy_2^-}{2\pi} \theta(y_1^- - y_2^-)\theta(-y^-)\frac{1}{xp^+}\langle p_A | F^{\sigma+}(y_2^-)F_\alpha^{+}(0)F^{+\alpha}(y_1^-)F_\sigma^{+}(y^-)|p_A\rangle. \tag{13b}$$

In Eq. (13), $F_{\mu\nu}$ and ψ_q are the field strength and quark field operators, respectively. We have suppressed three path-ordered exponentials of the gauge field in each of the four-parton matrix elements in Eq. (13). These path-ordered exponentials sandwiched between field operators are necessary to make these matrix elements manifestly gauge invariant [13].

In Eq. (11), the H_i are the partonic hard parts, and

$$H_{q\bar{q}} = \left(\frac{2}{27}\right)\left(\frac{-u}{x's+u} + \frac{x's+u}{-u}\right), \tag{14a}$$

$$H_g = \left(\frac{1}{36}\right)\left(\frac{x's}{x's+u} + \frac{x's+u}{x's}\right), \tag{14b}$$

$$H_q = \left(\frac{1}{16}\right)\left(\frac{x's}{-u} + \frac{-u}{x's}\right), \tag{14c}$$

which we will derive in next section.

Equations (11), (12), and (14) are our complete analytic results at leading nonvanishing order in α_s. As usual, the next-to-leading order (NLO) contribution might be important for single and/or double scatterings. However, since the nuclear dependence parameter $\alpha(l)$, defined in Eq. (7), depends on the ratio of the double and single scattering contributions, we expect that the values of $\alpha(l)$ presented in this paper are not very sensitive to the NLO contributions.

III. DERIVATION OF THE DOUBLE SCATTERING CONTRIBUTIONS

In this section we provide the derivation that leads to the analytic results presented in the last section. The method that we used here was first introduced in Ref. [5]. It can be summarized in the following technical steps: (a) Factorize the double scattering contribution into a convolution between the partonic hard parts and the corresponding multiparton matrix elements [e.g., see Eq. (5)]; (b) in the leading pole approximation, integrate over two of the three independent momentum fractions by contour integrations, and reexpress the multiparton matrix elements in terms of the $T_q(x,A)$ and $T_g(x,A)$ defined in Eq. (13); (c) calculate the corresponding partonic hard parts.

At lowest order, only *three* types of partonic subprocesses, as sketched in Fig. 3, contribute to the double scattering cross section $d\sigma_{aA\to\gamma}^{(D)}$ introduced in Eq. (5). These three subprocesses correspond to adding two gluons to the lowest-order ''annihilation'' and ''Compton'' subprocesses, shown in Fig. 1. In the following subsections, we present the detailed derivation for one subprocess, and provide the results for other subprocesses.

A. Perturbative factorization

Consider the subprocess shown in Fig. 3(a), in which there are *three* independent *four-momentum* linking the partonic part and a corresponding two-quark–two-gluon matrix

element. In the center-of-mass frame of high-energy collision, all partons inside the nucleus are moving almost parallel to each other, along the direction of the nucleus. Therefore, all *three* parton momenta can be approximately replaced by components collinear to the hadron momentum. After such a collinear expansion, the double scattering contribution from the generalized ''annihilation'' subprocess shown in Fig. 3(a) can be written as [5]

$$E_l \frac{d\sigma_{qA\to\gamma}^{(D)}}{d^3 l} = \frac{1}{2x's} \int dx dx_k dx_{k'} \int d^2 k_T \overline{T}(x, x_k, x_{k'}, k_T, p) \overline{H}(x'p', x, x_k, x_{k'}, k_T, p, l), \tag{15}$$

where $2x's$ is the flux factor between the incoming beam quark and the nucleus, and $x'p'$ is the momentum carried by the beam quark. In Eq. (15), the two-quark–two-gluon matrix element $\overline{T}$ is defined as

$$\overline{T}(x, x_k, x_{k'}, k_T, p) = \int \frac{dy_1^-}{2\pi} \frac{dy_2^-}{2\pi} \frac{dy^-}{2\pi} \frac{d^2 y_T}{(2\pi)^2} e^{ixp^+ y_1^-} e^{ix_k p^+ y^-} e^{-i(x_k - x_{k'})p^+ y_2^-} e^{-ik_T \cdot y_T}$$

$$\times \frac{1}{2} \langle p_A | A^+(y_2^-, 0_T) \overline{\psi}_q(0) \gamma^+ \psi_q(y_1^-) A^+(y^-, y_T) | p_A \rangle. \tag{16}$$

The corresponding partonic part $\overline{H}$ is given by the diagrams shown in Fig. 4, with gluon lines contracted with $p^\rho p^\sigma$, quark lines from the target traced with $(\gamma \cdot p)/2$, and quark lines from the beam traced with $[\gamma \cdot (x'p')]/2$. Here, we work in the Feynman gauge, in which the leading contribution from the gluon field operators is $A^\rho \approx A^+(p^\rho/p^+)$. We also kept the k_T for the gluons in order to extract a double scattering contribution beyond the leading twist.

By expanding the partonic part $\overline{H}$ introduced in Eq. (15) at $k_T = 0$, we have

$$\overline{H}(x'p', x, x_k, x_{k'}, k_T, p, l) = \overline{H}(x'p', x, x_k, x_{k'}, k_T = 0, p, l) + \frac{\partial \overline{H}}{\partial k_T^\alpha} \bigg|_{k_T = 0} k_T^\alpha + \frac{1}{2} \frac{\partial^2 \overline{H}}{\partial k_T^\alpha \partial k_T^\beta} \bigg|_{k_T = 0} k_T^\alpha k_T^\beta + \cdots. \tag{17}$$

In the right-hand side of Eq. (17), the first term is the leading twist eikonal contribution, which does not correspond to physical double scattering, but simply makes the single scattering matrix element gauge invariant. The second term vanishes after integrating over k_T. The third term will give a finite contribution to the multiple scattering process. Substituting Eq. (17) into Eq. (15), and integrating over $d^2 k_T$, we obtain

$$E_l \frac{d\sigma_{qA\to\gamma}^{(D)}}{d^3 l} = \frac{1}{2x's} \int dx dx_k dx_{k'} T(x, x_k, x_{k'}, A) \left(-\frac{1}{2} g^{\alpha\beta} \right) \left[\frac{1}{2} \frac{\partial^2}{\partial k_T^\alpha \partial k_T^\beta} \overline{H}(x'p', x, x_k, x_{k'}, k_T = 0, p, l) \right], \tag{18}$$

where the modified matrix element T is given by

$$T(x, x_k, x_{k'}, A) = \int \frac{dy_1^-}{2\pi} \frac{dy^-}{2\pi} \frac{dy_2^-}{2\pi} e^{ixp^+ y_1^-} e^{ix_k p^+ y^-} e^{-i(x_k - x_{k'})p^+ y_2^-} \frac{1}{2} \langle p_A | F_\alpha^+(y_2^-) \overline{\psi}_q(0) \gamma^+ \psi_q(y_1^-) F^{+\alpha}(y^-) | p_A \rangle. \tag{19}$$

In Eq. (19), $F^{+\alpha} = F^{\beta\alpha} n_\beta$, $F^{\beta\alpha}$ is the field strength, and the vector $n_\beta = \delta_{\beta+}$.

In following sections, we show how to perform integrations over parton momentum fractions, and evaluate the partonic parts $(\partial^2/\partial k_T^\alpha \partial k_T^\beta) \overline{H}$ for different subprocesses.

B. Leading pole approximation

The double scattering contribution defined in Eq. (18) depends on integrations over three partonic momentum fractions x, x_k, $x_{k'}$. If all partons in Fig. 4 carry some finite momentum fractions, the oscillations of the exponentials in the matrix element T defined in Eq. (19) will destroy any nuclear size enhancement that could come from the y integrations. However, even at the lowest order, we find that there are some Feynman diagrams which have two poles corresponding to zero momentum fraction partons, and these poles are not pinched. Therefore, two of the three parton momentum fractions can be integrated explicitly by contour integration. These integrations will eliminate two exponentials, and thus the corresponding y integration could provide the nuclear size enhancement up to $A^{2/3}$. But in terms of the double scattering picture, if we require two soft field operators to come from the same nucleon, we will get the familiar $A^{1/3}$ enhancement.

Of course, there are double scattering diagrams without such poles, but we expect an A^α ($\alpha > 1$) dependence only when the poles are present. In this paper, we evaluate only diagrams that have such poles, and we call our results at the leading pole approximation.

In order to perform the integration of momentum fractions, it is convenient to rewrite the double scattering contribution defined in Eq. (18) as

$$E_l \frac{d\sigma_{qA\rightarrow\gamma}^{(D)}}{d^3l} = \frac{1}{2x's} \int \frac{dy_1^-}{2\pi} \frac{dy^-}{2\pi} \frac{dy_2^-}{2\pi} \frac{1}{2} \langle p_A | F_\alpha^{+}(y_2^-) \bar{\psi}_q(0) \gamma^+ \psi_q(y_1^-) F^{+\alpha}(y^-) | p_A \rangle \left(-\frac{1}{2} g^{\alpha\beta} \right)$$

$$\times \left[\frac{1}{2} \frac{\partial^2}{\partial k_T^\alpha \partial k_T^\beta} H(y_1^-, y^-, y_2^-, k_T=0, p, l) \right]. \tag{20}$$

In Eq. (20), the modified partonic part H is defined as

$$H(y_1^-, y^-, y_2^-, k_T, p, l) = \int dx dx_k dx_{k'} e^{ixp^+ y_1^-} e^{ix_k p^+ y^-} e^{-i(x_k - x_{k'})p^+ y_2^-} \bar{H}(x'p', x, x_k, x_{k'}, k_T, p, l), \tag{21}$$

where the partonic part $\bar{H}$ is given by diagrams shown in Fig. 4. It is clear from Eq. (21) that all integrals of momentum fractions can now be done explicitly without knowing the details of the multiparton matrix elements.

Consider the diagram shown in Fig. 4(a). The final-state photon-gluon two-particle phase space can be written as

$$\Gamma = \frac{1}{8\pi^2} \frac{1}{x's+u} \delta\left(x + x_k + \frac{x't}{x's+u} + \frac{-k_T^2 - 2k_T \cdot l}{x's+u} \right). \tag{22}$$

In deriving Eq. (22), we have omitted the factor d^3l/E_l, due to the definition of the invariant cross section [e.g., see Eq. (20)]. Using Eq. (22), the contribution to $\bar{H}$ from the diagram shown in Fig. 4(a) can be expressed as

$$\bar{H}_{I(a)} = \frac{\alpha_s}{2\pi} C_I \frac{1}{x's+u} \hat{H}_{I(a)}(x, x_k, x_{k'}) \frac{1}{x_k - x_{k'} - k_T^2/x's - i\epsilon} \frac{1}{x_k - k_T^2/x's + i\epsilon} \delta\left(x + x_k + \frac{x't}{x's+u} + \frac{-k_T^2 - 2k_T \cdot l}{x's+u} \right), \tag{23}$$

where the subscript I(a) has the following convention: ''I'' stands for the type-I subprocess, shown in Fig. 3(a); ''a'' for the real contribution, corresponding to diagrams in Fig. 4(a). In Eq. (23), the factor C_I is an overall color factor for the type-I subprocess. The function $\hat{H}_{I(a)}$ in Eq. (23) is given by

$$\hat{H}_{I(a)} = \frac{1}{4} \frac{1}{x's} \text{Tr}[\gamma \cdot (x'p' + k_T) \gamma \cdot p \gamma \cdot (x'p' + k_T) R_{I(a)}^{\beta\nu} \gamma \cdot p L_{I(a)}^{\alpha\mu}](-g_{\alpha\beta})(-g_{\mu\nu}), \tag{24}$$

where $R_{I(a)}^{\beta\nu}$ and $L_{I(a)}^{\alpha\mu}$ are the right and left blobs, respectively, as shown in Fig. 4(a). These blobs include all possible tree Feynman diagrams with the external partons shown in the figure. Substituting Eq. (23) into Eq. (21), we obtain

$$H_{I(a)} = \frac{\alpha_s}{2\pi} C_I \frac{1}{x's+u} \int dx_k e^{ix_k p^+ (y^- - y_2^-)} \frac{1}{x_k - k_T^2/x's + i\epsilon} \int dx_{k'} e^{ix_{k'} p^+ y_2^-} \frac{1}{x_k - x_{k'} - k_T^2/x's - i\epsilon}$$

$$\times \int dx e^{ixp^+ y_1^-} \delta\left(x + x_k + \frac{x't}{x's+u} + \frac{-k_T^2 - 2k_T \cdot l}{x's+u} \right) \hat{H}_{I(a)}(x, x_k, x_{k'}). \tag{25}$$

After performing dx_k and $dx_{k'}$ by contour integration, and dx by the δ function, we derive

$$H_{I(a)} = (2\pi\alpha_s) C_I \frac{1}{x's+u} e^{i\bar{x}p^+ y_1^-} e^{i(k_T^2/x's)p^+(y^- - y_2^-)} \theta(-y_2^-) \theta(y_1^- - y^-) \hat{H}_{I(a)}(\bar{x}, x_k, x_{k'}), \tag{26}$$

where the θ functions result from the contour integrations, and the momentum fractions for the function $\hat{H}_{I(a)}$ are defined as

$$\bar{x} = -\frac{1}{x's+u} \left[x't + \frac{u}{x's} k_T^2 - 2k_T \cdot l \right], \tag{27a}$$

$$x_k = \frac{k_T^2}{x's}, \tag{27b}$$

$$x_{k'} = 0, \tag{27c}$$

$$x = -\frac{x't}{x's+u}. \tag{27d}$$

Similarly, we derive contribution from the diagram shown in Fig. 4(b) as

$$H_{I(b)} = (2\pi\alpha_s)C_I\frac{1}{x's+u}e^{ixp^+y_1^-}e^{i(k_T^2/x's)p^+(y^--y_2^-)}\theta(y_2^--y^-)\theta(y_1^--y_2^-)\hat{H}_{I(b)}(x,x_k,x_{k'}), \tag{28}$$

where x, x_k, and $x_{k'}$ are also defined in Eq. (27). Similarly to Eq. (24), the partonic part $\hat{H}_{I(b)}$ is given by

$$\hat{H}_{I(b)} = \frac{1}{4}\text{Tr}[\gamma\cdot(x'p')R_{I(b)}^{\beta\nu}\gamma\cdot pL_{I(b)}^{\alpha\mu}](-g_{\alpha\beta})(-g_{\mu\nu}). \tag{29}$$

The diagram shown in Fig. 4(c) has the contribution

$$H_{I(c)} = (2\pi\alpha_s)C_I\frac{1}{x's+u}e^{ixp^+y_1^-}e^{i(k_T^2/x's)p^+(y^--y_2^-)}\theta(y^--y_2^-)\theta(-y^-)\hat{H}_{I(b)}(x,x_k,x_{k'}). \tag{30}$$

In deriving Eq. (30), we used the fact that the partonic part $\hat{H}_{I(c)} = \hat{H}_{I(b)}$ when x_k and $x_{k'}$ are evaluated at the same values as listed in Eq. (27).

Combining $H_{I(a)}$, $H_{I(b)}$, and $H_{I(c)}$ [given in Eqs. (26), (28), and (30), respectively] together, we obtain the total contribution to H, defined in Eq. (21), from the type-I diagrams shown in Fig. 3(a):

$$H_I = H_{I(a)} + H_{I(b)} + H_{I(c)}$$

$$= (2\pi\alpha_s)C_I\frac{1}{x's+u}e^{i(k_T^2/x's)p^+(y^--y_2^-)}\theta(-y_2^-)\theta(y_1^--y^-)[e^{i\bar{x}p^+y_1^-}\hat{H}_{I(a)}(\bar{x},x_k,x_{k'})-e^{ixp^+y_1^-}\hat{H}_{I(a)}(x,x_k,x_{k'})]. \tag{31}$$

All momentum fractions in Eq. (31) are evaluated at the values defined in Eq. (27). In deriving Eq. (31), we have dropped a term proportional to

$$[\theta(-y_2^-)\theta(y_1^--y^-)-\theta(y_2^--y^-)\theta(y_1^--y_2^-)-\theta(y^--y_2^-)\theta(-y^-)]\to 0.$$

This is because of the phase $\exp[ixp^+y^-]$ which effectively restricts $y_1^-\sim 1/(xp^+)\to 0$. Physically, it means that all y integrations in such term are localized and therefore will not give any large nuclear size enhancement.

By substituting Eq. (31) into Eq. (20), we can obtain the lowest-order double scattering contribution from the type-I diagrams shown in Fig. 3(a). One important step in getting the final result is taking the derivative with respect to k_T as defined in Eq. (20). Comparing Eq. (31) with Eq. (20), and observing that

$$[e^{i\bar{x}p^+y_1^-}\hat{H}_{I(a)}(\bar{x},x_k,x_{k'})-e^{ixp^+y_1^-}\hat{H}_{I(a)}(x,x_k,x_{k'})]_{k_T=0}=0, \tag{32}$$

we found that the derivatives on the exponential $\exp[i(k_T^2/x's)p^+(y^--y_2^-)]$ do not contribute, and that we can therefore set $\exp[i(k_T^2/x's)p^+(y^--y_2^-)]=1$ in Eq. (31). Substituting Eq. (31) into Eq. (20), and use Eq. (13a), we obtain

$$E_l\frac{d\sigma_I^{(D)}}{d^3l} = \alpha_{em}(4\pi\alpha_s)^2e_q^2C_I\frac{1}{2x's}\frac{1}{x's+u}\left(-\frac{1}{2}g^{\alpha\beta}\right)\frac{1}{2}\frac{\partial^2}{\partial k_T^\alpha\partial k_T^\beta}[T_q(\bar{x},A)\hat{H}_{I(a)}(\bar{x},x_k,x_{k'})-T_q(x,A)\hat{H}_{I(b)}(x,x_k,x_{k'})], \tag{33}$$

where $\sigma_I^{(D)}$ stands for the double scattering contribution from the type-I subprocess shown in Fig. 3(a). It is important to note that although the interference diagrams shown in Fig. 4(b) and Fig. 4(c) are important in driving Eq. (33), the final result depends only on the real diagram shown in Fig. 4(a). That is, the double scattering picture is preserved. The role of interference diagrams is to take care of the infrared sensitivities of the short-distance hard parts.

C. Final factorized form

The derivatives with respect to k_T in Eq. (33) are straightforward. It is most convenient to reexpress derivatives with respect to k_T in terms of derivatives with respect to $\bar{x}$ or x. After working out the derivatives, we obtain [5]

$$E_l\frac{d\sigma_I^{(D)}}{d^3l} = \alpha_{em}(4\pi\alpha_s)^2e_q^2\frac{1}{2x's}\frac{1}{x's+u}H_{q\bar{q}}2\left\{\left[\frac{\partial^2}{\partial x^2}\left(\frac{T_q(x,A)}{x}\right)\right]\left(\frac{l_T^2}{(x's+u)^2}\right)+\left[\frac{\partial}{\partial x}\left(\frac{T_q(x,A)}{x}\right)\right]\left(\frac{-u}{x's(x's+u)}\right)\right\}, \tag{34}$$

where x is given in Eq. (27d), and where the partonic hard part $H_{q\bar{q}}$ is defined as

$$H_{q\bar{q}} = C_I x\hat{H}_{I(a)}(x,x_k=0,x_{k'}=0). \tag{35}$$

Following the same derivation, we obtain contributions from the type-II and type-III diagrams shown in Fig. 3. For the type-II diagrams, as sketched in Fig. 3(b), we have

$$E_l \frac{d\sigma_{\text{II}}^{(D)}}{d^3 l} = \alpha_{\text{em}}(4\pi\alpha_s)^2 e_q^2 \frac{1}{2x's} \frac{1}{x's+u} H_g 2 \left\{ \left[\frac{\partial^2}{\partial x^2} \left(\frac{T_g(x,A)}{x} \right) \right] \left(\frac{l_T^2}{(x's+u)^2} \right) + \left[\frac{\partial}{\partial x} \left(\frac{T_g(x,A)}{x} \right) \right] \left(\frac{-u}{x's(x's+u)} \right) \right\}. \quad (36)$$

In Eq. (36), the partonic hard part H_g is defined as

$$H_g = C_{\text{II}} \hat{H}_{\text{II(a)}}(x, x_k = 0, x_{k'} = 0), \quad (37)$$

where C_{II} is the overall color factor for the type-II diagrams, and $\hat{H}_{\text{II(a)}}$ is given by the real diagrams shown in Fig. 5, and defined as

$$\hat{H}_{\text{II(a)}} = \frac{1}{4} \text{Tr}[\gamma \cdot (x'p' + x_k p + k_T) R_{\text{II(a)}}^{\beta\nu} \gamma \cdot l' L_{\text{II(a)}}^{\alpha\mu}](-g_{\alpha\beta})(-g_{\mu\nu}), \quad (38)$$

where $l' = x'p' + (x + x_k)p - l$ is the momentum carried by the quark going to final state. Similarly, for the type-III diagrams, as sketched in Fig. 3(c), we obtain

$$E_l \frac{d\sigma_{\text{III}}^{(D)}}{d^3 l} = \alpha_{\text{em}}(4\pi\alpha_s)^2 e_q^2 \frac{1}{2x's} \frac{1}{x's+u} H_q 2 \left\{ \left[\frac{\partial^2}{\partial x^2} \left(\frac{T_q(x,A)}{x} \right) \right] \left(\frac{l_T^2}{(x's+u)^2} \right) + \left[\frac{\partial}{\partial x} \left(\frac{T_q(x,A)}{x} \right) \right] \left(\frac{-u}{x's(x's+u)} \right) \right\}. \quad (39)$$

The partonic hard part H_q in Eq. (39) is defined as

$$H_q = C_{\text{III}} x \hat{H}_{\text{III(a)}}(x, x_k = 0, x_{k'} = 0), \quad (40)$$

where C_{III} is the overall color factor for the type-III diagrams, and $\hat{H}_{\text{III(a)}}$ is given by the real diagrams shown in Fig. 6, and defined as

$$\hat{H}_{\text{III(a)}} = \frac{1}{4} \text{Tr}[\gamma \cdot p R_{\text{III(a)}}^{\beta\nu} \gamma \cdot l' L_{\text{III(a)}}^{\alpha\mu}](-g_{\alpha\beta})(-g_{\mu\nu}), \quad (41)$$

where l' is the same as that defined after Eq. (38).

The partonic short-distance hard parts, defined in Eqs. (35), (37), and (40), can be easily evaluated by calculating the corresponding Feynman diagrams. Our results were presented in Eq. (14) in Sec. II B.

After convoluting Eqs. (34), (36), and (39) with the corresponding parton distributions from the beam, we obtain the complete analytical expressions for the double scattering contribution in hadron-nucleus collisions, which was presented in Eq. (11) of Sec. I B.

IV. NUMERICAL RESULTS AND DISCUSSIONS

In this section, we present our numerical results for the Cronin effect in direct photon production. We numerically evaluate the nuclear dependence parameter $\alpha(l)$ defined in Eq. (7) by using our analytical results presented in Eqs. (8) and (11), and we also compare our numerical results with recent data from Fermilab experiment E706 [6].

The nuclear dependence parameter $\alpha(l)$ defined in Eq. (7) depends on contributions from both single scattering and double scattering. All these contributions depend on nonperturbative parton distributions or multiparton correlation functions. In deriving the following numerical results, the set 1 pion distributions of Ref. [14] are used for pion beams, and the CTEQ3L parton distributions of Ref. [9] are used for free nucleons. The twist-4 multiparton correlation functions defined in Eq. (13) have not been well measured yet. By com-

paring the definition of these twist-4 correlation functions with the normal twist-2 parton distributions [15], the authors of Ref. [5] proposed the following approximate expressions for the twist-4 correlation functions:

$$T_i(x,A) = \lambda^2 A^{1/3} f_{i/A}(x,A), \qu(42)$$

where $i = q$, $\bar{q}$, and g. The $f_{i/A}$ are the effective twist-2 parton distributions in nuclei, and the factor $A^{1/3}$ is proportional to the size of nucleus. The constant λ^2 has dimensions of $[\text{energy}]^2$ due to the difference between twist-4 and twist-2 matrix elements. The value of λ^2 was estimated in Ref. [16] by using the *measured* nuclear enhancement of the momentum imbalance of two jets in photon-nucleus collisions [17,18], and was found to be

$$\lambda^2 \sim 0.05 - 0.1 \text{ GeV}^2. \quad (43)$$

This value is not too far away from the naive expectation from the dimensional analysis, $\lambda^2 \sim \Lambda_{\text{QCD}}^2$. In our calculation below, we use $\lambda^2 = 0.1 \text{ GeV}^2$. Therefore, our numerical results can be thought as the upper limit of the theoretical predictions.

The $A^{1/3}$ dependence of the twist-4 multiparton correlation functions, introduced in Eq. (42), is not unique. From the definition of the correlation functions in Eq. (13), the lack of oscillation factors for both y^- and y_2^- integrals can in principle give nuclear enhancement proportional to $A^{2/3}$. The $A^{1/3}$ dependence is a result of the assumption that the positions of two field strengths (at y^- and y_2^-, respectively) are confined within one nucleon.

In Eq. (42), the effective nuclear parton distributions $f_{i/A}$ should have the same operator definitions of the normal parton distributions with free nucleon states replaced by the nuclear states. For a nucleus with Z protons and atomic number A, we define

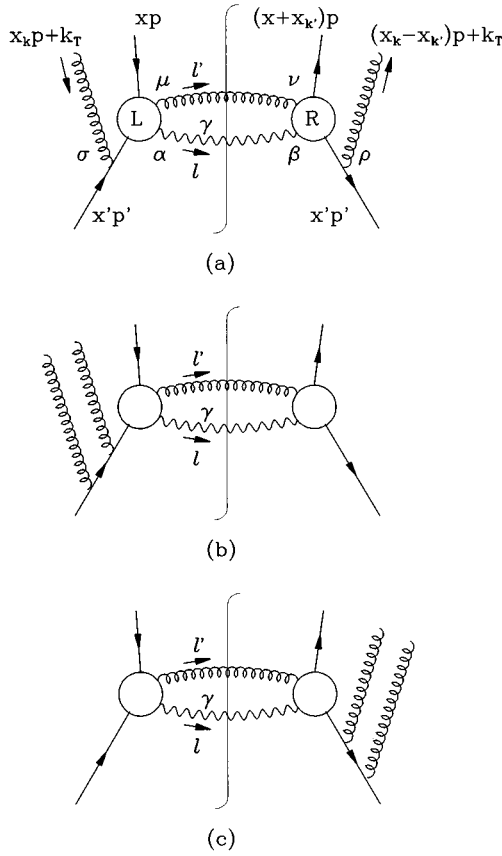$$f_{i/A}(x,A) = A \left(\frac{N}{A} f_{i/N}(x) + \frac{Z}{A} f_{i/P}(x) \right) R_i^{\text{EMC}}(x,A), \qu(44)$$

FIG. 4. Feynman diagrams for the "annihilation" diagrams corresponding to the two-quark–two-gluon matrix element: (a) real diagrams, and (b) and (c) interference diagrams.

where $f_{i/N}(x)$ and $f_{i/P}(x)$ with $i = q, \bar{q}, g$ are normal parton distributions in a free neutron and proton, respectively, and $N = A - Z$. The factor R_i^{EMC} takes care of the EMC effect in these effective nuclear parton distributions. We adopted the R^{EMC} from Ref. [19], which fits the data well. However, at fixed target energies, the x values covered by direct photon experiments are large and out of the nuclear shadowing region. The integration over dx' in Eqs. (8) and (11) averages out the EMC effect from the large x region. Actually, one can neglect the R_i^{EMC} in Eq. (44).

Using the parton distributions and correlation functions introduced above, and our analytic results presented in Eqs. (8) and (11), we can derive the nuclear dependence parameter $\alpha(l)$, defined in Eq. (7), *without* any further free parameter.
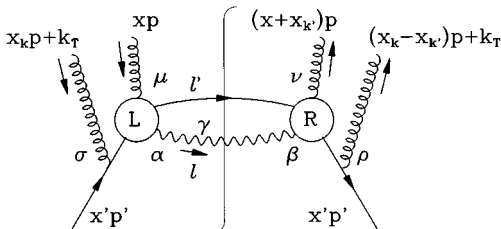

FIG. 5. The real "Compton" diagrams corresponding to the four-gluon matrix element.
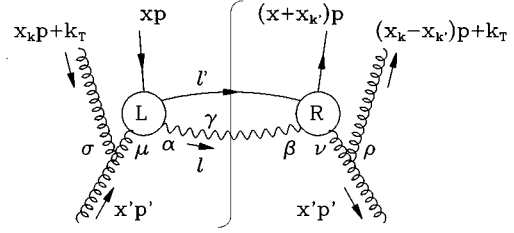

FIG. 6. The real "Compton" diagrams corresponding to the two-quark–two-gluon matrix element.

In Fig. 7, we compare our numerical predictions for the nuclear dependence parameter with recent experimental data from the Fermilab experiment E706 [6]. The $\alpha_{\mathrm{E706}}(l)$ presented in Fig. 7 is slightly different from that defined in Eq. (7). E706 measured the direct photon cross sections with the π^- beam on two different targets $\mathrm{Cu}(A = 63.55)$ and $\mathrm{Be}(A = 9.01)$, and the $\alpha_{\mathrm{E706}}(l)$ was extracted according to the definition

$$\frac{\sigma_{\mathrm{Cu}}(l)}{\sigma_{\mathrm{Be}}(l)} \equiv \left(\frac{A_{\mathrm{Cu}}}{A_{\mathrm{Be}}} \right)^{\alpha_{\mathrm{E706}}(l)}. \tag{45}$$

The beam energy is $p' = 515$ GeV. It is clear that the theoretical calculation presented in this work is consistent with the data.

It is evident from Fig. 7 that the nuclear dependence parameter $\alpha_{\mathrm{E706}}(l)$ is very close to unity or, equivalently, the Cronin effect for direct photon production is very small, and much smaller than that observed in the single particle inclusive cross sections [1]. One clear difference between the direct photon and the single particle inclusive cross sections is that direct photon production has only initial-state multiple scattering, while the single particle inclusive has both initial-
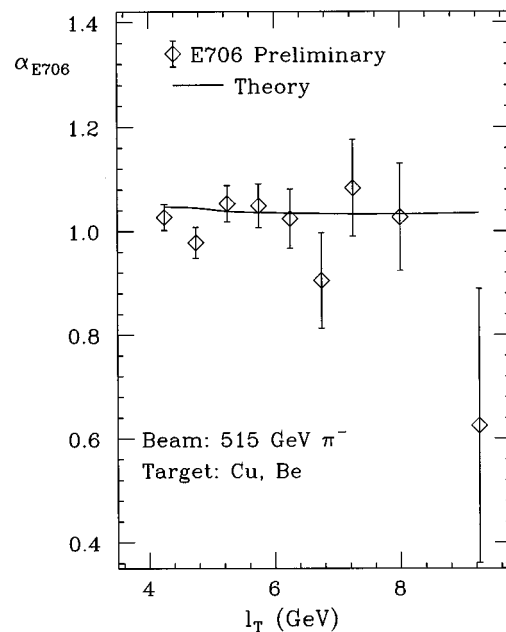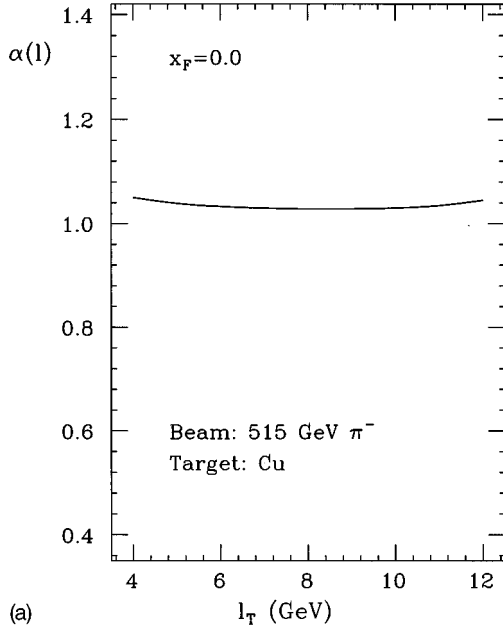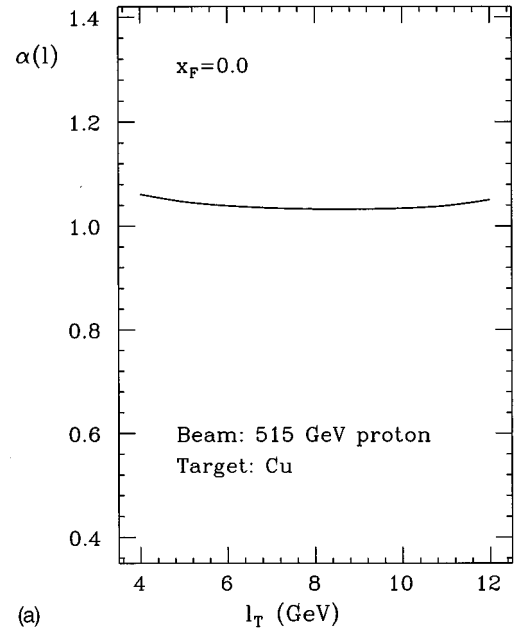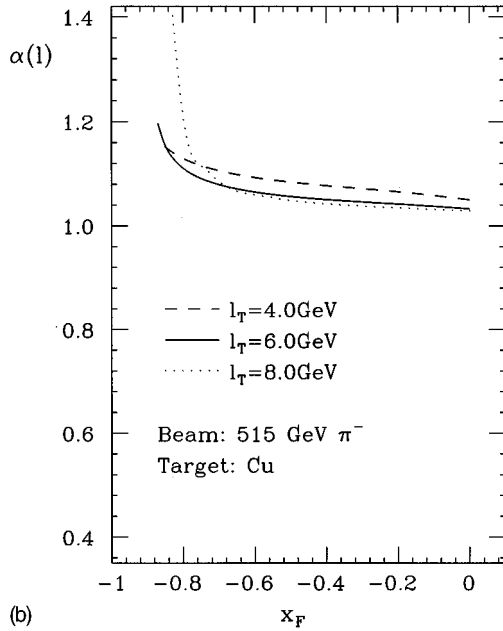

FIG. 7. Cronin effect in direct photon production with 515 GeV π^- beam on Cu and Be targets. The theory curve is from Eq. (45), and the data are from Fermilab experiment E706 [6].
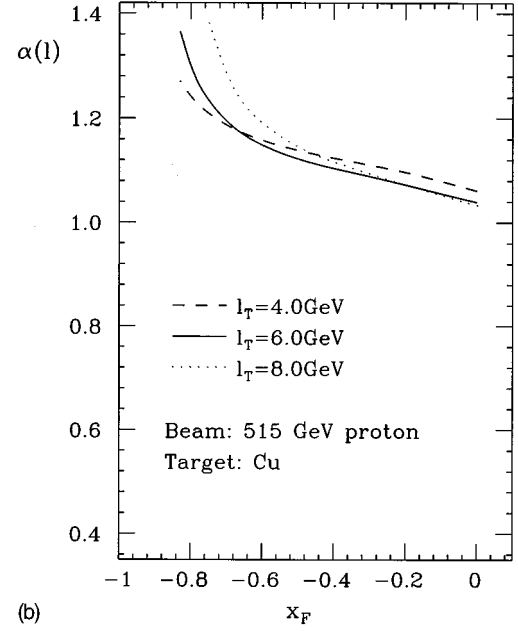
FIG. 8. Theoretical predictions of $\alpha(l)$ of Eq. (7): (a) as a function of the photon's transverse momentum at $x_F = 0.0$; (b) as a function of x_F at $l_T = 4.0$, 6.0, and 8.0 GeV, respectively. A 515 GeV π^- beam and copper target were used.

FIG. 9. Theoretical predictions of $\alpha(l)$ of Eq. (7), as in Fig. 8, but with a proton beam.

and final-state multiple scattering. In addition, the single particle inclusive cross sections depend on the parton-to-hadron fragmentation functions.

As pointed out in Ref. [5], the multiple scattering contribution is most important when the momentum fraction x from the nuclear correlation functions is large because of the derivatives with respective to the x, which were introduced in Eq. (12). However, for direct photon production, the kinematics do not fix all parton momentum fractions, and leave one momentum fraction to be integrated, for example, x' in Eqs. (8) and (11). Because of the steeply falling nature of the

distributions and correlation functions, the cross sections in the central region ($x_F \sim 0$) for a given value of l_T are dominated by the distributions with momentum fractions $x' \sim x \sim x_T = 2l_T / \sqrt{s}$, which are less than 0.6 even for the largest value of l_T shown in Fig. 7. Therefore, the double scattering contribution is relatively small because the derivative terms are not significantly enhanced, and consequently, $\alpha_{E706}(l)$ is close to one.

In contrast, for inclusive single hadron production, the parton-to-hadron fragmentation functions effectively shift the contribution at a given l_T to the large x region because all fragmentation functions vanish when z goes to 1. Kinematically, direct photon production corresponds to single particle production at $z = 1$. We therefore expect that single hadron

production has a larger Cronin effect than direct photon production at the exact same kinematics, even before including contributions of final-state multiple scattering.

In the case of a pion beam, the quark-antiquark ''annihilation'' subprocess, sketched in Fig. 1(a), dominates the production of direct photons at the fixed target energy, due to valence antiquarks in the beam. However, for a proton beam, the quark-gluon ''Compton'' subprocess, as sketched in Fig. 1(b), is more important for the production of direct photons. Therefore, direct photon production with a proton beam is more sensitive to proton gluon distributions. In Figs. 8, and 9, we present our predictions of the nuclear dependence parameter $\alpha(l)$, defined in Eq. (7), for a π^- and proton beam, respectively.

In Figs. 8(a) and 9(a), the nuclear dependence parameter $\alpha(l)$, defined in Eq. (7), is plotted as a function of the photon transverse momentum l_T at $x_F=0$. In plotting these figures, a 515 GeV beam energy and a copper target were assumed, using the same parton distributions and correlation functions as in Fig. 7. As expected, and as found in Fig. 7, the value of $\alpha(l)$ is very close to one for both pion and proton beams. Changing a pion beam by a proton beam does not affect the kinematics of the collisions. The effective values of parton momentum fractions from the nuclear target are the same for both cases. Therefore, as explained above, the values of $\alpha(l)$ are close to one due to the fact that the effective parton momentum fractions from the nuclear target are not large.

In order to enhance the contribution from the double scattering, we need to look for events at large negative x_F, where the effective values of parton momentum fractions from the target are larger. In Figs. 8(b) and 9(b), we plot the nuclear dependence parameter $\alpha(l)$, defined in Eq. (7), as a function of x_F at $l_T=4.0$, 6.0, and 8.0 GeV, respectively. The same beam, target, and beam energy were used. It is clear that when x_F becomes large and negative, $\alpha(l)$ increases. This is consistent with the fact that the larger the negative values of x_F, the larger the effective values of parton momentum fractions from the nuclear target and, consequently, the larger the derivatives, defined in Eq. (12).

The nuclear dependence calculated in this paper is known as a power correction (or a ''high-twist'' effect) to the normal single scattering. As one would expect, the ratio of double scattering over the single scattering is proportional to $1/l_T^2$, which vanishes as l_T^2 increases. However, because of the derivatives with respect to x in Eq. (12), the ratio effectively has three types of terms proportional to $1/l_T^2$, $1/[(1-x)l_T^2]$, and $1/[(1-x)^2l_T^2]$, respectively. For fixed values of x, all three terms vanish as $1/l_T^2$. However, in our case, the values of x and l_T^2 are not independent. When the effective values of x from the target partons are small, all three types of terms should show $1/l_T^2$ behavior. This is clearly evident in Figs. 8(b) and 9(b): For a fixed value of $x_F\sim0$, $\alpha(l_T)$ decreases as l_T increases. However, as x_F decreases, the effective values of x increase much faster for the situation with a larger value of l_T due to the phase space limit. As a result, the term proportional to $1/(1-x)^2l_T^2$ becomes more important than the $1/l_T^2$ term. Therefore, it is possible that the nuclear dependence is larger for a larger l_T, when the effective values of x are near 1. Such a feature is evident in Figs. 8(b) and 9(b) when x_F is very negative. Of course, when $\alpha_s/(1-x)^2l_T^2$ is of order of one, we will have to take into account all higher-power terms [20].

Comparing Figs. 8(b) and 9(b), one finds that as x_F decreases, the values of $\alpha(l)$ with a proton beam increase much faster than that with a pion beam. This is because the Compton subprocess dominates the production of direct photons in the case of a proton beam, and the gluon distribution in a proton falls much faster than valence quark distributions as the momentum fraction increases. The more rapidly falling gluon distribution produces larger derivative terms, and therefore, larger values of $\alpha(l)$. Future data from Fermilab experiment E706 with a proton beam can test this feature.

In summary, using generalized factorization in QCD perturbation theory, and using the method, developed in Ref. [5], for calculating nuclear enhancements, we demonstrated in this paper that the observed small Cronin effect in direct photon production is consistent with the much larger Cronin effect observed in single jet and single particle inclusive cross sections. We hope that the same method can be used to explain the puzzle for the nuclear dependence in the momentum imbalance. Data on dijet momentum imbalance in photoproduction [17] and hadroproduction [18] have shown strong nuclear dependence, while a much smaller nuclear dependence has been seen in the momentum imbalance of Drell-Yan pairs [21].

ACKNOWLEDGMENTS

[1] J. W. Cronin et al., Phys. Rev. D **11**, 3105 (1975); L. Kluberg et al., Phys. Rev. Lett. **38**, 670 (1977); R. L. McCarthy et al., ibid. **40**, 213 (1978); D. Antreasyan et al., Phys. Rev. D **19**, 764 (1979); H. Jöstlein et al., ibid. **20**, 53 (1979).

[2] P. M. Fishbane and J. S. Trefil, Phys. Rev. D **12**, 2113 (1975); J. H. Kühn, ibid. **13**, 2948 (1976); M. J. Longo, Nucl. Phys. **B134**, 70 (1978); A. Krzywicki, J. Engels, B. Petersson, and U. Sukhatme, Phys. Lett. **85B**, 407 (1979); V. V. Zmushko, Yad. Fiz. **32**, 246 (1980) [Sov. J. Nucl. Phys. **32**, 127 (1980)].

[3] M. Lev and B. Petersson, Z. Phys. C **21**, 155 (1983); K. Kastella, G. Sterman and J. Milana, Phys. Rev. D **39**, 2586 (1989).

[4] E. M. Levin and M. G. Ryskin, Yad. Fiz. **47**, 1397 (1988) [Sov. J. Nucl. Phys. **47**, 889 (1988)]; G. T. Bodwin, S. J. Brodsky, and G. P. Lepage, Phys. Rev. D **39**, 3287 (1989).

[5] M. Luo, J. Qiu, and G. Sterman, Phys. Lett. B **279**, 377 (1992); Phys. Rev. D **50**, 1951 (1994).

[6] E706 Collaboration, M. Zieliński, in proceeding of the Conference on the Intersections of Nuclear and Particle Physics, St.

Petersburg, Florida, 1994 (AIP, New York, in press).

[7] J. F. Owens, Rev. Mod. Phys. **59**, 465, (1987), and references therein.

[8] P. Aurenche, R. Baier, M. Fontannaz, J. F. Owens, and M. Werlen, Phys. Rev. D **39**, 3275 (1989).

[9] H. L. Lai *et al.*, Phys. Rev. D **51**, 4763 (1995), and references therein.

[10] A. D. Martin, R. G. Roberts, and W. J. Stirling, Phys. Rev. D **50**, 6734 (1994), and references therein.

[11] J. C. Collins, D. E. Soper, and G. Sterman, in *Perturbative Quantum Chromodynamics*, edited by A. H. Mueller (World Scientific, Singapore, 1989).

[12] E. L. Berger and J. Qiu, Phys. Rev. D **44**, 2002 (1991).

[13] J. Qiu and G. Sterman, Nucl. Phys. **B353**, 105 (1991); **B353**, 137 (1991).

[14] J. F. Owens, Phys. Rev. D **30**, 943 (1984).

[15] J. C. Collins and D. E. Soper, Nucl. Phys. **B194**, 445 (1982).

[16] M. Luo, J. Qiu, and G. Sterman, Phys. Rev. D **49**, 4493 (1994).

[17] D. Naples *et al.*, Phys. Rev. Lett. **72**, 2341 (1994).

[18] M. D. Corcoran *et al.*, Phys. Lett. B **259**, 209 (1991); T. Fields, Nucl. Phys. **A544**, 565 (1992).

[19] C. J. Benesh, J. Qiu, and J. P. Vary, Phys. Rev. C **50**, 1015 (1994).

[20] S. J. Brodsky, P. Hoyer, A. H. Mueller, and W.-K. Tang, Nucl. Phys. **B369**, 519 (1992).

[21] M. L. Swartz *et al.*, Phys. Rev. Lett. **53**, 32 (1984); D. M. Alde *et al.*, *ibid.* **66**, 2285 (1991).